

Single-Atom Implanted Two-dimensional MOFs as Efficient Electrocatalysts for Oxygen Evolution Reaction

Rui-Li Peng^a, Jia-Luo Li^b, Xiao-Ning Wang^a, Yu-Meng Zhao^a, Bao Li^{a,*}, Bao Yu
Xia,^{a,*}and Hong-Cai Zhou^{b,c,*}

^a *Key Laboratory of Material Chemistry for Energy Conversion and Storage, School of Chemistry and Chemical Engineering, Huazhong University of Science and Technology, Wuhan, Hubei, 430074, PR China. E-mail: libao@hust.edu.cn.*

^b *Department of Chemistry, Texas A&M University, College Station, Texas 77843-3255, United States.*

^c *Department of Materials Science and Engineering, Texas A&M University, College Station, Texas 77842, United States.*

Experimental details

Materials. All reagents are used directly after purchase from commercial sources without further purification.

Preparation of HUST-8. First of all, at the bottom 20 ml tube, in turn, add solution (16 mg ligand, 5 ml methylene chloride), central solution (4 ml of ethanol, 2 ml DMF), the upper solution (24 mg ferric chloride, 5 mg ascorbic acid, 5 ml of methanol), using the sealing membrane seal, quiet place, room temperature diffusion 15 days or so, in contact with ligand Fe^{2+} and generate purple flake HUST-8.

Preparation of Fe@HUST-8, Co@HUST-8, Ni@HUST-8, Mn@HUST-8, Zn@HUST-8. With 10mg HUST-8 as the template, 7.2mg ferrous chloride ($\text{FeCl}_2 \cdot 4\text{H}_2\text{O}$), 13.62mg cobalt chloride ($\text{CoCl}_2 \cdot 6\text{H}_2\text{O}$), 14mg nickel chloride ($\text{NiCl}_2 \cdot 6\text{H}_2\text{O}$), 16mg manganese chloride ($\text{MnCl}_2 \cdot 4\text{H}_2\text{O}$), and 9mg zinc chloride (ZnCl_2) were added into 100mL chloroform, respectively. After overnight reflux, they were washed with water, ethanol and acetonitrile, centrifugated and dried in a oven at 85°C .

X-Ray Structural Determination. Diffraction data for HUST-7 has been collected via Bruker Venture using $\text{Cu-K}\alpha$ ($\lambda = 1.54178 \text{ \AA}$) radiation at 100 K. The structures of complexes were solved by direct methods, and the non-hydrogen atoms were located from the trial structure and then refined anisotropically with SHELXTL using a full-matrix leastsquares procedure based on F^2 values. The hydrogen atom positions were fixed geometrically at calculated distances and allowed to ride on the parent atoms. Attempts to define the highly disordered solvent molecules were unsuccessful, so the structure was refined with the PLATON “SQUEEZE” procedure. The diffraction intensity of crystal sample was very weak due to the very small size and large porous framework, which must be responsible for the corresponding alert A. CCDC-2011238 for the data under different temperature contain the supplementary crystallographic data for this paper. The data can be obtained free of charge from The Cambridge Crystallographic Data Centre via http://www.ccdc.cam.ac.uk/data_request/cif (or from the Cambridge Crystallographic

Data Centre, 12 Union Road, Cambridge CB2 1EZ, U.K.). The details for structural analyses of the HUST-5 and HUST-7 were listed in Table S1-3.

Characterizations. The morphology was observed with a Sigma HD Thermal field emission scanning electron microscope (SEM). Powder X-ray diffraction (PXRD) was carried out on a Bruker D8-Focus Bragg-Brentano X-ray Powder Diffractometer equipped with a Cu sealed tube ($\lambda = 1.54178 \text{ \AA}$) at 40 kV and 40 Ma, the data were analyzed with JADE. The elemental composition of the samples were characterized by energy-dispersive X-ray spectroscopy (EDS, Oxford instruments X-Max). The X-ray photoelectron spectroscopy (XPS) spectras were collected by Thermo ESCALAB 250XI spectrometer. Thermogravimetry analysis (TGA) was conducted on a TGA-50 thermogravimetric analyzer.

Electrochemical measurements and products analysis. Electrochemical testing was carried out in 1M KOH electrolyte using standard CHI760E electrochemical workstation with three electrodes. Glass carbon electrode (GCE) with diameter of 3mm was used as the working electrode, Pt network as the counter electrode, and Hg/HgO electrode as the reference electrode.

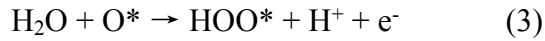
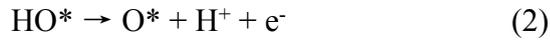
Preparation of catalyst dispersion solution. 5mg catalyst was dispersed in the mixed solution of 0.955mL ethanol and 0.005 ml5% Nafion, and ultrasonic treatment was conducted for 30min to form uniform dispersion solution. Then, The 10 μ L catalyst drops onto the polished GCE. To evaluate OER performance, a linear scan voltammetry curve (LSV) with a scan rate of 5mVs is obtained, from which the Tafel slope is obtained. Electrochemical impedance spectroscopy (EIS) in the range of 100000 ~0.1Hz was analyzed. When the current density was 10mA cm⁻², the stability of the catalyst was tested by chronopotentiometry method.

Computational Details

All density functional theory (DFT) calculation were carried out using the Vienna ab initio simulation package (VASP) ¹. The Perdew-Burke-Ernzerhof (PBE) functional with the generalized gradient approximation (GGA), accounting for inhomogeneous charge-density distributions, was used to describe the exchange-

correlation effect in Kohn-shame equation. Projector-augmented wave (PAW) method, featuring the accuracy of all-electron method and the efficiency of pseudopotential method, was used to treated inner core and valent electrons. The cutoff energy of 400 eV is set to expansion of plane wave function basic set. The K-point of the Brillouin zone sampled by the Monkhorst-Pack method was set to $1 \times 1 \times 1$ grid with Γ -pointer center, having enough accuracy for all calculation cluster models. In order to get accurate weak interaction between reaction species and catalyst, the Van der Waals correction method (DFT-D3) was adopted for all self-consistent field calculations. The initial structures of cluster model were derived from single-crystal diffraction with vacuum layer of 15.0 Å to avoid the interaction of two periodic images.

Electrocatalytic oxygen evolution reaction consists of four elementary steps, as following:



In this work, we adopt the standard hydrogen electrode (SHE) . That means the free energy of H^+/e^- pairs is equal to that of $1/2 \text{H}_2$ in the gas phase at standard conditions ($p = 1 \text{ bar}$, $T = 298.15 \text{ K}$, $\text{pH} = 0$, $U = 0$) . The Gibbs free energies (ΔG) for each elemental step in accordance with the method of the Nørskov et al, was calculated by:

$$\Delta G_0 = \Delta E_{\text{DFT}} + \Delta \text{ZPE} - T\Delta S \quad \text{Eq (5)}$$

where E is the reaction energy using DFT calculation. ZPE and S are the zero point energy and entropy, which are calculated via DFT calculation of the vibrational frequencies and using standard tables for gas-phase molecules respectively. T is set to

298.15 K in this work. Under the applied electrode potential U condition, the Gibbs free energy can be written as:

$$G_U = G_0 - neU \quad \text{Eq(6)}$$

where n is the number of the transferred electron and U is the electrode potential relative to the SHE.

The overpotential (η) is typically evaluated by following formula:

$$\eta = U_L - U_{\text{equilibrium}} \quad \text{Eq(7)}$$

where $U_{\text{equilibrium}}$ is the equilibrium potential. The equilibrium-potential is 1.23 V for 4e-mechanism. U_L , the highest potential for all of steps in free energy, is calculated by:

$$U_L = \Delta G/e \quad \text{Eq(8)}$$

where ΔG is the free energy of the potential-limiting step.

The adsorption energies (E_{ads}) of different adsorbates were calculated by :

$$E_{\text{ads}} = E_{\text{total}} - E_{\text{sub}} - E_{\text{mol}} \quad \text{Eq(9)}$$

where E_{total} , E_{sub} , E_{mol} are the total energy of slab after adsorption, bare catalyst, and the adsorbate molecule including the O, HO, HOO, H₂O, respectively.

Table S1. Crystal data and structure refinement for HUST-8.

	HUST-8
Empirical formula	C ₃₀ H ₃₀ ClFeN ₃
Formula weight	523.87
Temperature/K	100.01
Crystal system	monoclinic
Space group	<i>P2/c</i>

a/Å	14.2814(5)
b/Å	13.9589(5)
c/Å	16.7879(7)
α /°	90
β /°	97.534(2)
γ /°	90
Volume/Å ³	3317.8(2)
Z	4
ρ_{calc} /cm ³	1.049
μ /mm ⁻¹	4.518
Crystal size/mm ³	0.15 × 0.15 × 0.05
Final R indexes [$I \geq 2\sigma(I)$]	R ₁ = 0.1194, wR ₂ = 0.3336
Final R indexes [all data]	R ₁ = 0.1364, wR ₂ = 0.3505

Table S2. Bond Lengths for HUST-8.

Atom	Atom	Length/Å	Atom	Atom	Length/Å
Fe01	Cl02 ¹	2.4378(19)	C15	C19A	1.37(2)
Fe01	Cl02	2.4377(19)	C3	C6	1.450(10)
Fe01	N1	2.244(5)	C3	C2	1.410(8)
Fe01	N1 ¹	2.244(5)	C3	C4	1.438(12)
Fe01	N2 ²	2.229(5)	C3	C2A	1.402(10)
Fe01	N2 ³	2.229(5)	C3	C4A	1.46(3)
N1	C1	1.379(8)	C6	C7	1.426(9)
N1	C5	1.272(11)	C6	C20	1.341(9)
N1	C1A	1.399(10)	C11	C12	1.445(9)
N1	C5A	1.46(3)	C11	C10	1.388(11)
N5	C13	1.363(9)	C7	C8	1.457(10)

N5	C13 ⁴	1.363(9)	C13	C12	1.388(10)
N4	C7	1.380(8)	C13	C14	1.450(11)
N4	C7 ⁴	1.380(8)	C20	C9	1.416(9)
N2	Fe01 ⁵	2.229(5)	C9	C10	1.361(12)
N2	C17	1.420(16)	C8	C8 ⁴	1.437(14)
N2	C18	1.370(9)	C14	C14 ⁴	1.225(15)
N2	C17A	1.392(10)	C1	C2	1.320(13)
N2	C18A	1.34(2)	C4	C5	1.404(8)
N3	C11	1.345(8)	C1A	C2A	1.41(5)
N3	C20	1.406(8)	C4A	C5A	1.400(10)
C15	C12	1.488(9)	C16	C17	1.382(9)
C15	C16	1.423(16)	C18	C19	1.421(19)
C15	C19	1.390(9)	C16A	C17A	1.32(3)
C15	C16A	1.399(10)	C18A	C19A	1.404(10)

Asymmetric codes: ¹1-X,+Y,3/2-Z; ²+X,1+Y,+Z; ³1-X,1+Y,3/2-Z; ⁴-X,+Y,3/2-Z; ⁵+X,-1+Y,+Z

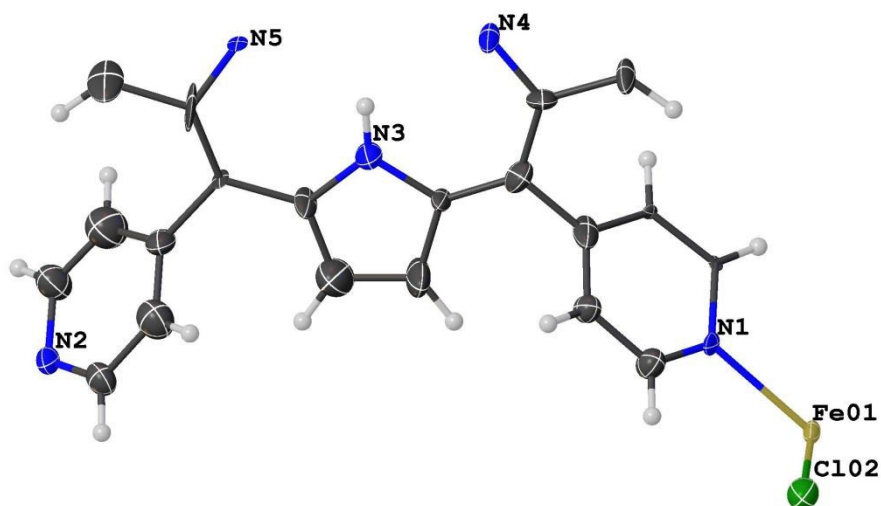


Figure S1. Asymmetric unit of HUST-8 along with atom labeling

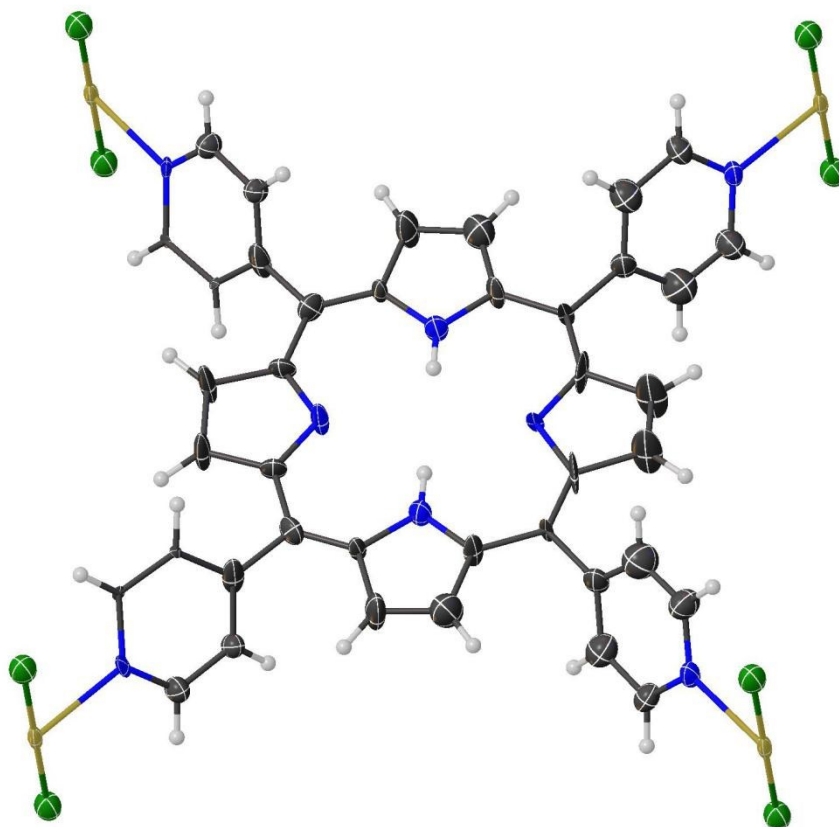
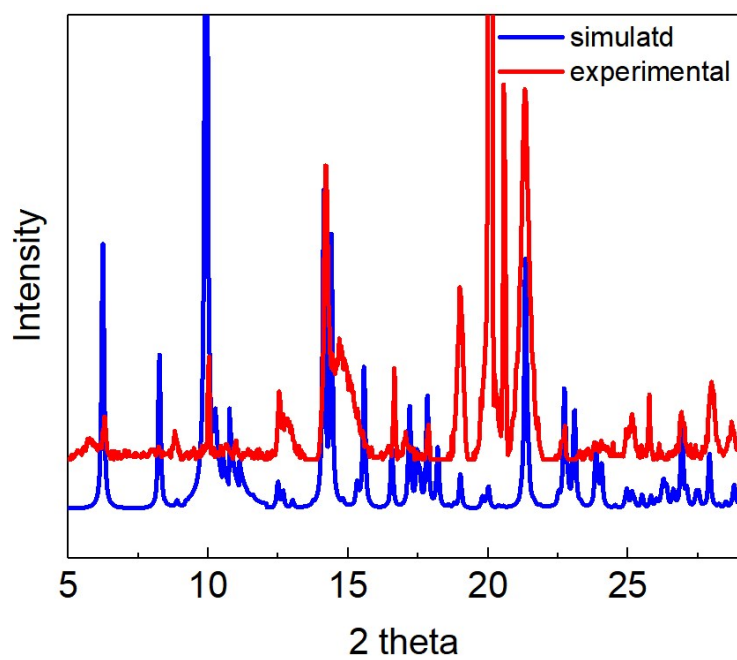


Figure S2. Partial view of the connection mode of tetrapyridinate ligand in HUST-8



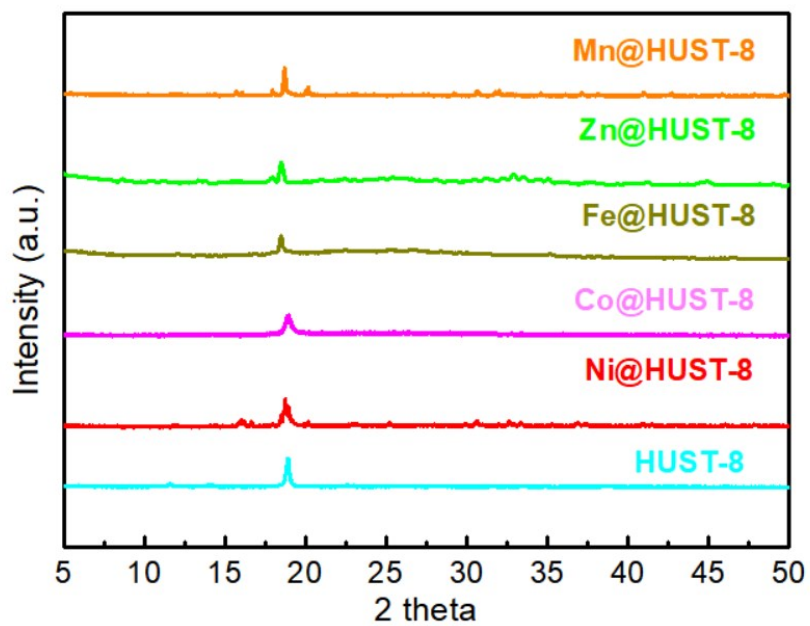


Figure S3. The XRD patterns of different samples.

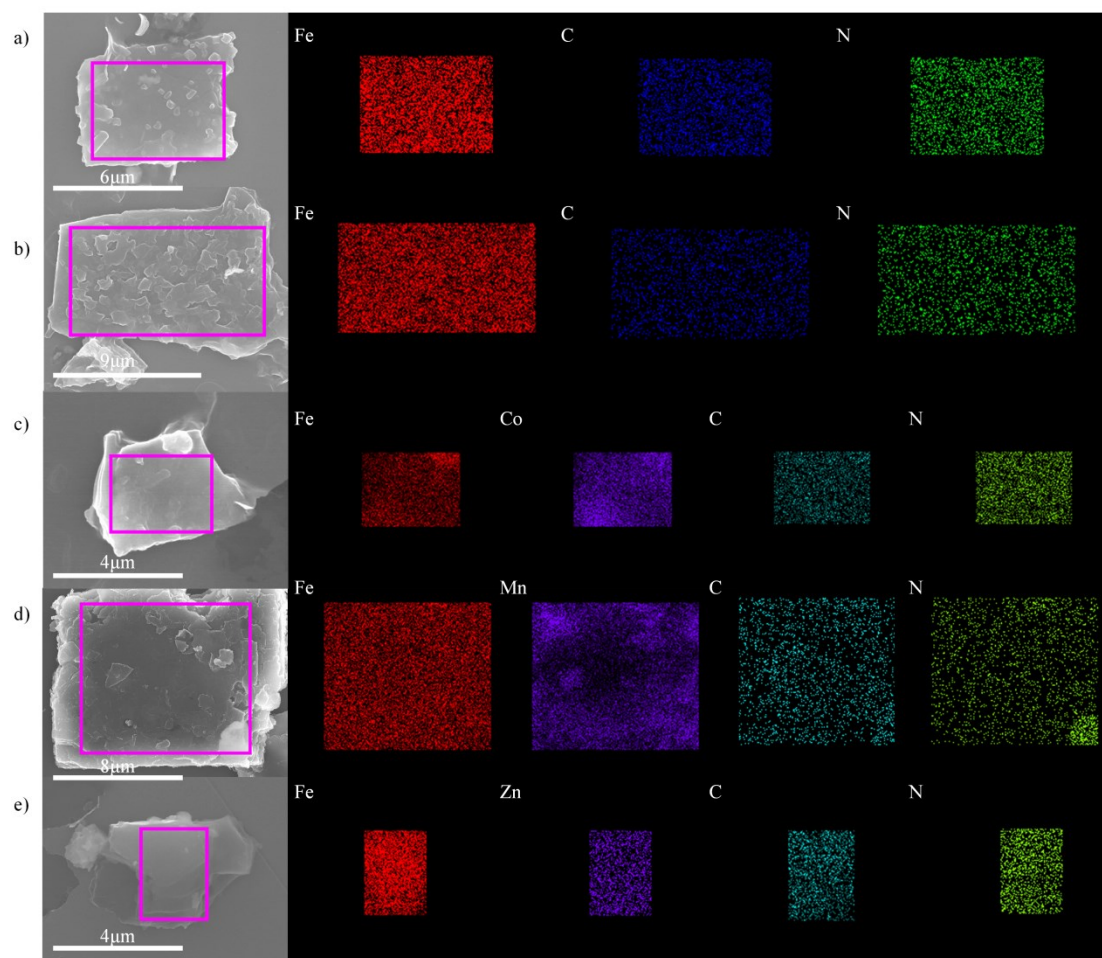


Figure S4. STEM-EDX elemental mapping of the (a) HUST-8; (b) Fe@HUST-8; (c) Co@HUST-8; (d) Mn@HUST-8; and (e) Zn@HUST-8.

Table S3. The ratio of secondary metal, Fe, and, Cl elements in different samples.

Samples	the ratio of secondary metal, Fe, and, Cl elements
HUST-8	0:1:1.85
Fe@HUST-8	1.17:1:1.99
Co@HUST-8	1.25:1:1.89
Ni@HUST-8	1.20:1:2.03
Mn@HUST-8	1.13:1:1.84
Zn@HUST-8	0.96:1:1.92

Table S4. The XPS peak value of Fe 2p in different samples.

Samples	Satellite peak 1 (eV)	Fe 2P _{1/2} (eV)	Satellite peak 2 (eV)	Fe 2P _{3/2} (eV)
HUST-8	728.55	722.98	714.12	709.98
Fe@HUST-8	729.09	724.15	714.47	710.73
Co@HUST-8	724.44	717.94	713.58	710.09
Ni@HUST-8	726.06	723.09	715.08	710.03
Mn@HUST-8	727.88	723.43	713.94	710.25
Zn@HUST-8	722.76	717.95	709.58	703.93
Ni@HUST-8 after catalysis	725.46	729.91	713.43	710.99

Table S5. The XPS peak value of N in different samples.

Samples	Pyrrrolic N (eV)	Pyridinic N (eV)
HUST-8	399.27	397.78
Fe@HUST-8	399.52	398.52
Co@HUST-8	399.61	398.32
Ni@HUST-8	399.64	398.91
Mn@HUST-8	399.43	398.49
Zn@HUST-8	399.65	398.04
Ni@HUST-8 after catalysis	399.40	397.99

Table S6. ICP results for different samples.

Samples	the ratio of secondary metal, Fe, and Cl elements
HUST-8	0:1:1.92
Fe@HUST-8	1:0.917
Co@HUST-8	1.18:1:1.86
Ni@HUST-8	1.23:1:1.89
Mn@HUST-8	1.09:1:2.07
Zn@HUST-8	1.26:1:1.79

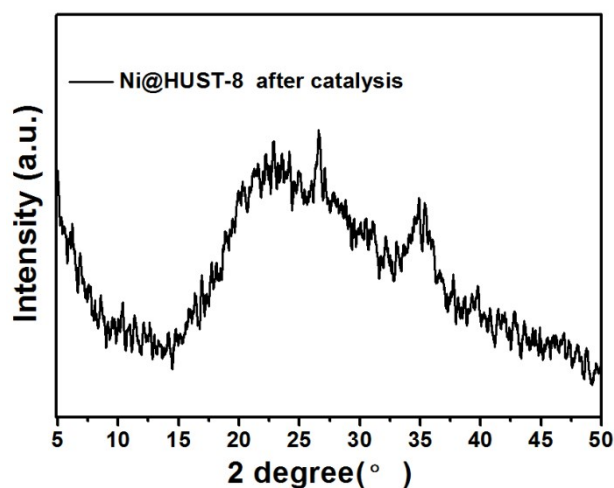


Figure S5. The XRD patterns of Ni@HUST-8 after catalysis.

Table S7. Comparison of the OER performance of the as-prepared catalysts with literature reports.

Catalysts	Overpotential V	Tafel slope mV dec ⁻¹	Reference
Ni@HUST-8	0.24	60.8	This work
CoO _x -ZIF	0.318	70.3	Adv.Funct. Mater., 2017, 27, 1702546.
NiFe-LDH-CNTs	0.25	31	J. Am. Chem. Soc. 135, 8452-8455 (2013)
UTSA-16	0.408	77	ACS Appl. Mater. Interfaces, 2017, 9, 7193.
NiFe@NCX	0.325	60.6	ACS Catal. 2016, 6, 6335–6342
NiCo-UMOFNs	0.25	42	Nat. Energy, 2016, 1, 16184
Ni ^{II} Fe ^{III} @NC	~0.258	60	Nano Energy, 2017, 39, 245–252
Fe/Ni _{2.4} /Co _{0.4} -MIL-53	0.219	53.5	Angew. Chem., Int. Ed., 2018, 57, 1888.
NiSe-Ni _{0.85} Se/CP	0.30	98	Small, 2018, 1800763

A2.7B-MOF-FeCo1.6	0.288	39	Adv. Energy Mater. 2018, 8, 1801564
-------------------	-------	----	-------------------------------------

Table S8. Details of TOF calculation

	$J/(\text{mA}/\text{cm}^2)@ \eta$ $=0.3\text{V}$	m/mol	A(cm^2)	F(C/mol)	TOF(S^{-1})
HUST-8	0.81	6.70745×10^{-8}	0.196	98465	0.00601
Fe@HUST	2.10	6.23994×10^{-8}	0.196	98465	0.01675
Co@HUST	25.04	6.23932×10^{-8}	0.196	98465	0.19972
Ni@HUST	90.54	6.24118×10^{-8}	0.196	98465	0.72192
Mn@HUST	3.99	6.24703×10^{-8}	0.196	98465	0.03178
Zn@HUST	10.79	6.16659×10^{-8}	0.196	98465	0.08707
IrO ₂	7.52	2.23015×10^{-7}	0.196	98465	0.01678

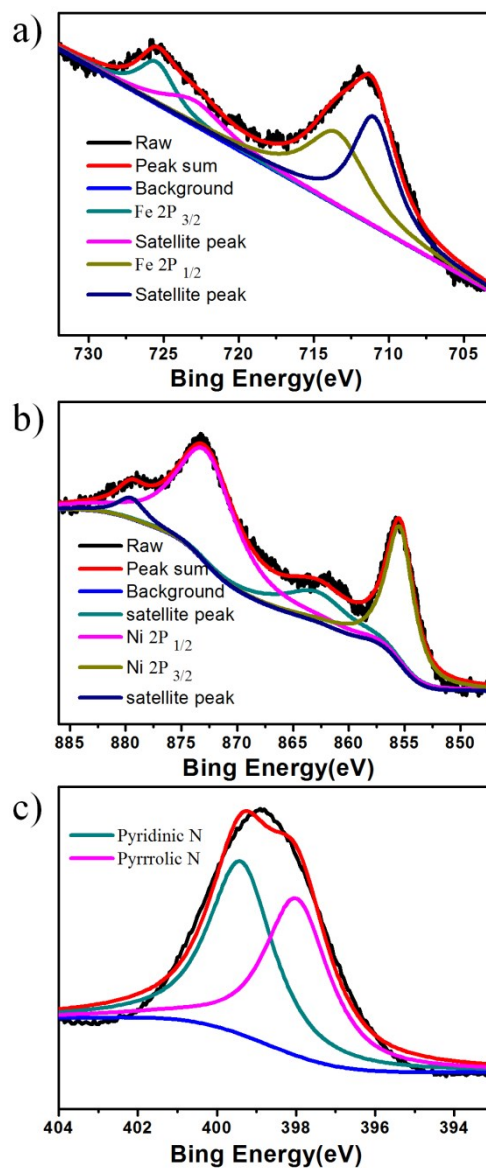


Figure S6. XPS patterns of the Ni@HUST-8 after catalysis. (a) Fe 2P scan XPS patterns, (b) Ni 2P scan XPS patterns, (c) N 1s scan XPS patterns.

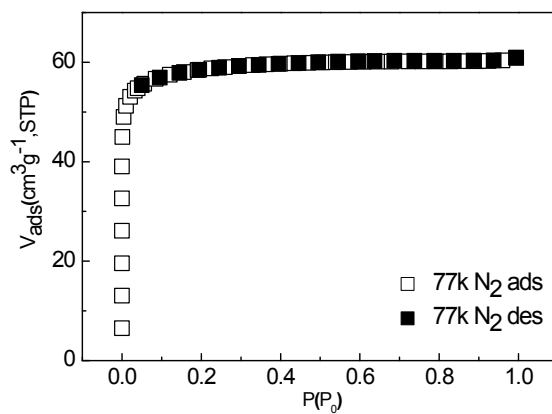


Figure S7. N₂ adsorption curves of HUST-8, which exhibits the reversible type-I isotherm and gives the values of Langmuir surface area of 240.3 m² g⁻¹ (BET surface area of 155.2 m² g⁻¹).

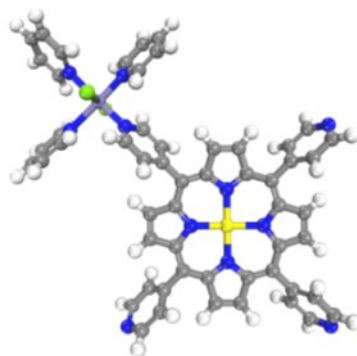


Figure S8. Optimized structure of Ni@HUST-8. (H white; C brown; N blue; Cl green; Ni yellow; Fe Light stone grey)

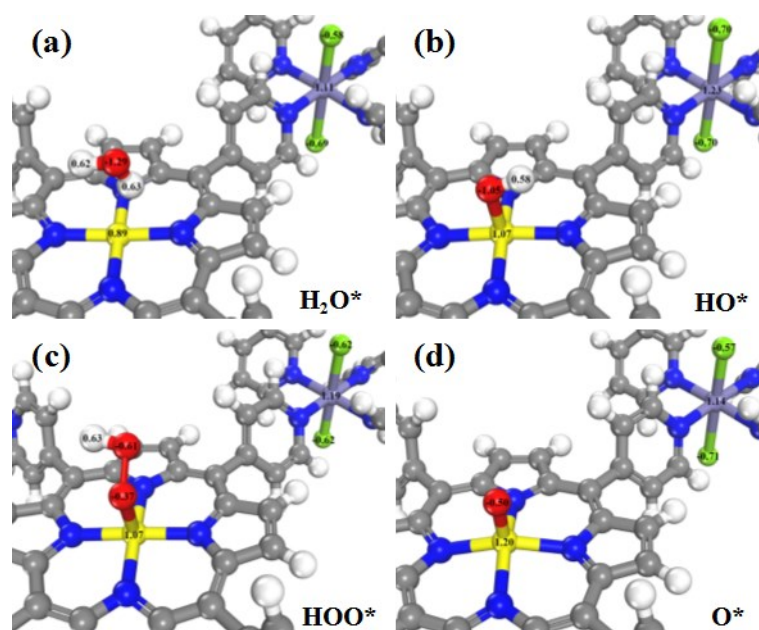


Figure S9. Bader charge of atom H, O, Cl, Ni, Fe in the four adsorption configuration (H white; C brown; N blue; O red; Cl green; Ni yellow; Fe Light stone grey)

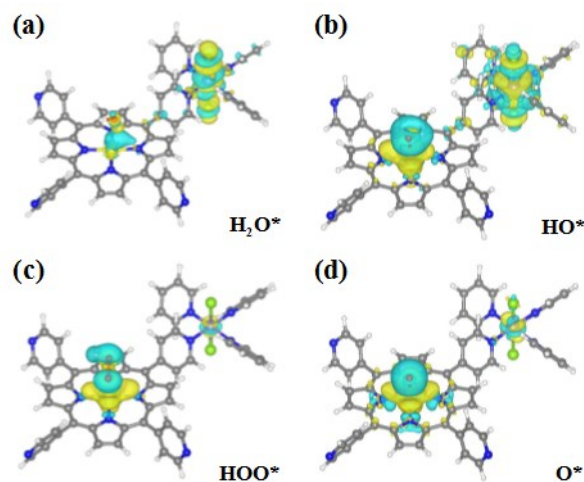


Figure S10. The corresponding Charge density difference values of atom H, O, Cl on Ni and Fe, respectively. (H white; C brown; N blue; O red; Cl green; Ni yellow; Fe Light stone grey)

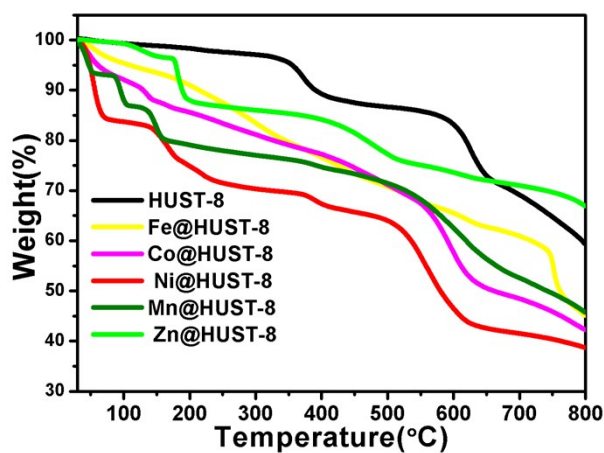


Figure S11. TGA curves of different samples

Notes and references

- [1]P. E. Blochl, Phys. Rev. B, 1994, 50, 17953-17979.
- [2]G. Kresse and J. Furthmuller, Comput. Mater. Sci., 1996, 6, 15-50.
- [3]G. Kresse and D. Joubert, Phys. Rev. B., 1999, 59, 1758-1775.

- [4]J. P. Perdew, K. Burke and M. Ernzerhof, Phys. Rev. Lett., 1996, 77, 3865-3868.
- [5]R. A. Evarestov and V. P. Smirnov, Phys. Rev. B., 2004, 70, 233101.
- [6]S. Grimme, J. Antony, S. Ehrlich and H. Krieg, J. Chem. Phys., 2010, 132, 154104.
- [7]J. K. Norskov, J. Rossmeisl, A. Logadottir, L. Lindqvist, J. R. Kitchin, T. Bligaard and H. Jonsson, J. Phys. Chem. B., 2004, 108, 17886-17892.
- [8]Vanderbilt, D. Phys. ReV. B 1990, 41, 7892.